

The Journal of Immunology

This information is current as
of November 6, 2010

**On How Monospecific Memory-Like
Autoregulatory CD8 + T Cells Can
Blunt Diabetogenic Autoimmunity: A
Computational Approach**

Anmar Khadra, Sue Tsai, Pere Santamaria and Leah
Edelstein-Keshet

J. Immunol. 2010;185:5962-5972; originally published
online Oct 20, 2010;
doi:10.4049/jimmunol.1001306
<http://www.jimmunol.org/cgi/content/full/185/10/5962>

**Supplementary
Data**

[http://www.jimmunol.org/cgi/content/full/jimmunol.1001306/D
C1](http://www.jimmunol.org/cgi/content/full/jimmunol.1001306/D
C1)

References

This article **cites 23 articles**, 13 of which can be accessed free
at:
<http://www.jimmunol.org/cgi/content/full/185/10/5962#BIBL>

Subscriptions

Information about subscribing to *The Journal of Immunology* is
online at <http://www.jimmunol.org/subscriptions/>

Permissions

Submit copyright permission requests at
<http://www.aai.org/ji/copyright.html>

Email Alerts

Receive free email alerts when new articles cite this article. Sign
up at <http://www.jimmunol.org/subscriptions/etoc.shtml>

On How Monospecific Memory-Like Autoregulatory CD8⁺ T Cells Can Blunt Diabetogenic Autoimmunity: A Computational Approach

Anmar Khadra,* Sue Tsai,[†] Pere Santamaria,^{†,1} and Leah Edelstein-Keshet^{‡,1}

We have recently shown that during progression to autoimmune diabetes in NOD mice, memory autoreactive regulatory CD8⁺ T cells arising from low-avidity precursors can be expanded to therapeutic levels using nanoparticles coated with disease-relevant peptide-major histocompatibility complexes (pMHCs). Here we examine the dynamics of memory autoregulatory CD8⁺ T cells specific for islet-specific glucose-6-phosphatase catalytic subunit-related protein_{206–214}, a prevalent β cell autoantigen; their high-avidity counterparts (dominant effectors); and all other autoreactive non-islet-specific glucose-6-phosphatase catalytic subunit-related protein_{206–214}-specific CD8⁺ T cell specificities (subdominant effectors) in response to pMHC-coated nanoparticle (pMHC-nanoparticle) therapy. We combine experimental data with mathematical modeling to investigate the clonal competition dynamics of these T cell pools. To mimic the response diversity observed in NOD mice, we simulated many individual mice, using a wide range of parameters, and averaged the results as done experimentally. We find that under certain circumstances, pMHC-nanoparticle-induced expansion of autoregulatory CD8⁺ T cells can effectively suppress the expansion of dominant and subdominant effectors simultaneously but, in some few cases, can lead to the substitution (or switching) of one effector population by another. The model supports the idea that disease suppression is based on the elimination of autoantigen-loaded APCs by the expanded autoregulatory CD8⁺ T cells. The model also predicts that treatment strategies that operate by selectively inhibiting autoantigen-loaded APCs, such as the pMHC-nanoparticle approach, have the highest promise to blunt polyclonal, multiantigen-specific autoimmune responses in vivo without impairing systemic immunity. *The Journal of Immunology*, 2010, 185: 5962–5972.

In humans and in NOD mice, the autoimmune form of type 1 diabetes (T1D) results from the destruction of pancreatic β cells by CD4⁺ and CD8⁺ T cells that target a multiplicity of Ags (1). Many of the CD8⁺ T cells in pancreatic islets of NOD mice recognize the mimotopes NRP-A7 and NRP-V7 in the context of the MHC molecule K^d (2–7). These diabetogenic T cells (6, 7) express a restricted set of TCR- α -chains (V α 17 and J α 42 elements joined by the amino acid sequence MRD) (4, 7, 8); target a peptide, islet-specific glucose-6-phosphatase catalytic subunit-related protein (IGRP_{206–214}), which resembles NRP-A7 and

NRP-V7 (9); and are found in circulation close to the clinical onset of the disease (9, 10). The diabetogenic CD8⁺ T cell response is polyclonal, involving recognition of many other epitopes (11), not only of IGRP but also of other β cell-specific autoantigens and T1D-associated Ags expressed on other cell types. For instance, a relatively small population within the islet CD8⁺ infiltrate recognizes MimA2/D^b, an agonistic mimic of the residues 138–146 of the protein dystrophin myotonia kinase (DMK_{138–146}).

Aside from the challenge created by this polyspecific response, clones with individual specificities are observed to engage peptide-major histocompatibility complexes (pMHCs) over a broad range of avidities. Pathogenic potential is known to correlate with the pMHC-binding avidity of a given T cell clone (12, 13). During progression of T1D, autoreactive CD8⁺ T cells undergo “avidity maturation,” a process shaped by tolerance and competition (8, 12). The competition between the prevalent nonpathogenic low-avidity clones and the rarer pathogenic higher-avidity clones (whether between or within antigenic specificities) helps us to understand why the diabetogenic autoimmune response progresses slowly relative to T cell dynamics in acute infections. A typical example of intraclonal competition occurs among IGRP_{206–214} specific V α 17-MRD-J α 42⁺ clonotypes using different V α 17 elements, such as the nonpathogenic low-avidity 17.6 α /8.3 β clone and the pathogenic higher-avidity 17.4 α /8.3 β clone (8).

This complexity is a challenge in the design of therapies. The goal of selectively purging the immune system of autoreactivity without immunologically compromising the patient is difficult to achieve. Ag-specific T cell tolerance can be induced by soluble peptides (14), but this strategy fails to curtail polyspecific autoimmune responses. For example, NRP-V7 therapy does not protect NOD mice from T1D, even though it effectively deletes the IGRP_{206–214}-specific CD8⁺ T cell pool. This treatment fosters occupation of the pre-

*Laboratory of Biological Modeling, National Institute of Diabetes and Digestive and Kidney Diseases, National Institutes of Health, Bethesda, MD 20892; [†]Department of Microbiology and Infectious Diseases, Julia McFarlane Diabetes Research Centre, Faculty of Medicine, University of Calgary, Calgary, Alberta; and [‡]Department of Mathematics, Institute of Applied Mathematics, University of British Columbia, Vancouver, British Columbia, Canada

¹P.S. and L.E.-K. contributed equally to this work and share senior authorship.

Received for publication April 21, 2010. Accepted for publication September 9, 2010.

This work was supported in part by the Mathematics of Information Technology and Complex Systems Canada and by the Juvenile Diabetes Research Foundation (to A.K.), a studentship from the Alberta Innovates-Health Solutions (to S.T.), the Canadian Institutes of Health Research, the Natural Sciences and Engineering Research Council of Canada, and the Juvenile Diabetes Research Foundation (to P.S.), as well as the Natural Sciences and Engineering Research Council of Canada (to L.E.-K.). L.E.-K. has been a 2009–2010 Distinguished Scholar in Residence at the Peter Wall Institute of Advanced Studies, University of British Columbia.

Address correspondence and reprint requests to Pere Santamaria, Julia McFarlane Diabetes Research Centre, Department of Microbiology and Infectious Diseases, Faculty of Medicine, University of Calgary, Calgary, Alberta, Canada T2N 4N1. E-mail address: psantama@ucalgary.ca

The online version of this article contains supplemental material.

Abbreviations used in this paper: CPM, counts per minute; DC, dendritic cell; IGRP, islet-specific glucose-6-phosphatase catalytic subunit-related protein; pMHC, peptide-major histocompatibility complex; pMHC-nanoparticles, pMHC-coated nanoparticles; T1D, type 1 diabetes.

viously occupied, now empty intra-islet “niche” by other pathogenic CD4⁺ and CD8⁺ T cell clonotypes.

To understand the complex clonal interactions and to provide rigorous platforms for testing hypotheses, we have constructed and analyzed a series of mathematical models in close contact with experimental data from our group (8, 15, 16). The first set of mathematical models exposed a complex relationship between pMHC avidity for cognate TCRs, peptide dose, and therapeutic effectiveness (15) and allowed us to explain counterintuitive predictions such as the observation that peptide therapy effectiveness is greater when it simultaneously promotes expansion of low-avidity (nonpathogenic) T cells as well as deletion of high-avidity clones. This suggested that therapeutic success might require deletion of multiple antigenic specificities, or the use of monospecific, T1D-relevant, altered peptide ligands of relatively low avidity.

More recently, we have evaluated the ability of nanoparticles coated with individual T1D-relevant pMHCs to induce tolerance of cognate autoreactive T cells. We reasoned that therapy with combinations of nanoparticles coated with different T1D-relevant pMHCs might allow the simultaneous deletion of several antigenic specificities without the extraordinarily high doses of peptides in solution needed for this purpose. Surprisingly, we found that therapy with monospecific pMHC-coated nanoparticles (pMHC-nanoparticles) could both blunt T1D progression in prediabetic mice and restore normoglycemia in newly diagnosed diabetic animals (17). Most surprisingly, we found that pMHC-nanoparticle therapy functions by expanding, in an epitope-specific manner, autoantigen-experienced autoreactive CD8⁺ cells that are not only devoid of pathogenic activity but also actually capable of suppressing the activation and recruitment of other autoantigenic specificities to the pancreas.

We showed that memory-like autoregulatory CD8⁺ cells arise spontaneously from nonpathogenic low-avidity autoreactive T cell clones during the progression of spontaneous disease and that they blunt the recruitment of other T cell specificities by suppressing Ag presentation in the pancreas-draining lymph nodes (17). The higher-avidity counterparts that give rise to these suppressive memory CD8⁺ T cells undergo terminal differentiation into cytolytic effectors that do not significantly accumulate as memory T cells. Because these newly discovered pools of protective low-avidity, Ag-experienced CD8⁺ T cells are not limited to specific epitopes or autoantigens and arise only in affected but not healthy individuals, we proposed that nanoparticles coated with any disease-relevant pMHC have the potential to become powerful vaccines capable of blunting and resolving polyclonal autoimmunity.

To understand the effects of pMHC-nanoparticle therapy on the diabetogenic immune response, we adapt our mathematical models for T cell competition to address experimental observations from pMHC-nanoparticle-treated mice. Specifically, we seek to address the following questions: 1) How does the competition among these different T cell pools influence the outcome of progression toward T1D? 2) How does expansion of the protective memory cell pool affect that outcome, and in particular, can it effectively dampen the activation and expansion of subdominant effectors? 3) How do realistic treatment scenarios (with distinct doses, timing, etc.) modulate the dynamics of competition among these different T cell pools? 4) Based on the above, how can treatment be optimized? In what follows, we explain the basis of the model and how we used it to address these questions.

Materials and Methods

Experimental and statistical methods

pMHC-nanoparticle treatment. pMHC-nanoparticles were synthesized as described in Ref. 17. Three different treatment schedules were implemented at three different disease stages. Three- to four-week-old female

NOD mice (at the stage where insulinitis first occurs) were treated with pMHC-nanoparticles in PBS at 7.5 μ g, 1.5 μ g, and 0.375 μ g iron equivalent i.v. every 2 wk until the third injection and every 3 wk thereafter (protocol 1, or standard treatment protocol). Prediabetic 10-wk-old NOD females were treated with 7.5 μ g iron equivalent pMHC-nanoparticles twice weekly until 12 wk of age (protocol 2) and 15 wk of age (protocol 3). New-onset diabetic NOD females (with whole-blood glucose exceeding 10.5 mM when checked with a glucometer [Accu-Chek Aviva; Roche, Laval, Quebec, Canada]) were treated with i.v. injections of 7.5 μ g iron equivalent pMHC-nanoparticles twice weekly (protocol 4) and every 2–3 wk (protocol 5) until stably normoglycemic for 4 consecutive wk. Mice were sacrificed 2 wk after the last injection. Peripheral blood was sampled after the last injection for flow cytometric analysis.

Culturing of pancreatic islet-derived T cells. Pancreatic islets were isolated as described in Ref. 7. Islet-associated CD8⁺ cells were obtained by culturing 10–50 islets/well in 24-well plates in RPMI 1640 medium supplemented with 10% FBS and 0.5 U/ml Takeda rIL-2 (18 ng/ml) for 6–10 d. Islet CD8⁺ responses toward a library of D^b- and K^d-restricted IGRP peptides (8) were assayed by coculturing gamma-irradiated NOD splenocytes (10⁵), individual peptides (1 μ M), and islet-derived CD8⁺ cells (2×10^4). Culture supernatants were collected at 48 h and assayed for IFN- γ by ELISA. Responses exceeding the lower limit of detection of 50 pg/ml IFN- γ were considered positive.

Assessment of T cell expansion. PE-conjugated TUM-H-2K^d and NRP-V7-H-2K^d tetramers were prepared as described in Ref. 2. Islet-derived T cells, PBMCs, and splenocytes were stained with tetramer (5 μ g/ml) in FACS buffer (0.1% sodium azide and 1% FBS in PBS) for 1 h at 4°C, washed, and incubated with FITC-conjugated anti-CD8 α (5 μ g/ml) and PerCP-conjugated anti-B220 (2 μ g/ml; as a “negative” channel, used to eliminate [gate out] nonspecifically stained cells from analysis) for 30 min at 4°C. Cells were washed, fixed in 1% paraformaldehyde/PBS, and analyzed by flow cytometry.

Comparing proliferative rates of high-avidity and low-avidity T cells. High-avidity effector cells were obtained by culturing 17.4 α /8.3 β -TCR-transgenic splenocytes with 1 μ g/ml NRP-V7 peptide for 3 d, followed by continued culture in RPMI 1640 supplemented with 10% FBS and 18 ng/ml IL-2 for 1 d. Low-avidity, 17.6 α /8.3 β -TCR-transgenic splenic CD8⁺ T cells enriched for the memory population were also used. Both cell types (2×10^4) were cultured with irradiated NOD splenocytes (10⁵, which serve as APCs) with a range of NRP-A7 peptide concentrations in IL-2-containing medium. [³H]Thymidine incorporation was determined for the period from 48 to 72 h of culture.

Statistical methods. Statistical analysis was performed with Mann–Whitney U test, and survival curves were compared using log-rank test. Data used for estimating treatment parameters are shown in Figs. 1 and 2 (see also Ref. 17 for more details).

Software. The model was analyzed by phase plane methods and linear stability and bifurcation methods (see supplementary material). Time-series simulations and bifurcation diagrams were generated using the software XPPAUTO (written by Bard Ermentrout and freely available online), and parameter estimations and population model analysis were conducted using MATLAB (Mathworks, Natick, MA).

Mathematical models

Our model (shown schematically in Fig. 4) follows the dynamics of three T cell types: IGRP_{206–214} (NRP-V7/K^d)-specific low-avidity autoregulatory CD8⁺ T cells (memory cells, denoted *M*), high-avidity IGRP_{206–214} (NRP-V7/K^d)-specific CD8⁺ T cells (dominant effectors, denoted *E*), and other autoreactive CD8⁺ T cells (subdominant effectors, denoted *Z*). Ordinarily, multiple specificities could be evoked in autoimmunity, and including *Z* allows us to investigate the possibility of subdominant clone invasion. T1D corresponds with elevated levels of *E* and/or *Z*.

All pools are assumed to contain some naive and memory cells for self-renewal. For simplicity, we restrict attention to two types of autoantigen released when β cells (population level *B*) are killed: *P*₁ represents IGRP_{206–214} (corresponding with *M* and *E* specificities), whereas *P*₂ depicts all other autoantigens lumped together into a single pool, to which cells of type *Z* are autoreactive. APCs are represented by the quantity *A*. The model is based on facts from T cell biology (*B*), experience from previous rounds of experiments and modeling (*E*), and new experimental data (*N*) as outlined below. Table I provides parameter values and meanings.

From basic T cell biology, we use the following facts:

- B1) Each T cell clone is produced by the thymus (rate $\bar{\sigma}_i$) and turns over (at rate δ_i). Memory cells are typically long-lived compared with effectors.

- B2) Activation (and proliferation) of a given clone depends on Ag levels and on the presence of APCs, predominately dendritic cells (DCs). Although B cells and macrophages also participate in autoantigen presentation, we focus on DCs due to their role in nanoparticle therapy.
- B3) Dominant effector T cells have greater peptide affinity, requiring less peptide for activation.

From our own previous experience with models and experiments (8, 15–19), we garner the following reasonable assumptions:

- E1) Input of naive cells from the thymus is roughly constant ($\bar{\sigma}_m \approx \bar{\sigma}_e \approx \bar{\sigma}_z$). We have shown in Ref. 16 that the impact of such terms is minimal by comparison with other processes.
- E2) T cell competition is well described by a term proportional to the total lymphocyte pool size, with the same competition parameter (\bar{e}) for each clone. Full discussion in Refs. 15 and 20 shows that this is required to prevent competitive exclusion.
- E3) The peptide-dependence for T cell activation is well approximated by a saturating sigmoidal (Hill) function; that is, clonal proliferation is negligible at low level of Ag, rises steeply beyond some threshold of Ag level, and levels off at high Ag level (15). We denote the functions for that peptide dependence by $\bar{f}_i(P_j)$ ($i = m, e, z$ and $j = 1, 2$).
- E4) Dominant and subdominant effector T cells, E and Z , kill β cells, whereas memory cells, M , are protective. Extensive evidence for this comes from previous experiments (8, 17).
- E5) Autoantigenic peptides are produced whenever β cells are killed and are gradually removed. \bar{R}_i denotes the peptide release rate per effector cell per β cell killed. A reasonable approximation for the peptide removal is first-order kinetics with rate constant δ_{p_j} (16, 19).
- E6) On the timescale of T cell expansion, autoantigen levels change rapidly and track the levels of β cells, whereas the latter change relatively slowly (15, 16, 21).
- E7) A roughly constant source (σ_a) of DCs is normally balanced by first-order turnover with rate δ_a . We also considered a possible rate of suppression (inactivation, or deletion) of DCs by direct action of low-avidity memory T cells. Evidence for this effect is found in Ref. 17, showing increased lysis of DCs pulsed with NRP-V7 and MimA2 when cocultured with low-avidity memory T cells.
- E8) The model has to account for the fact that some NOD mice remain healthy whereas others develop T1D.

To address specific observations on nanoparticle experiments, we made the following adaptations:

- N1) Clonal expansion depends on APCs. Evidence for this assumption is given in Fig. 3A, showing a decrease in the polyclonal IGRP-autoreactive CD8⁺ responses within the islets in NRP-V7/K^d- and MimA2/D^p-nanoparticle-treated mice (where APCs are suppressed) compared with those of control-nanoparticle-treated mice (where autoantigen-loaded APCs are present and functional, thereby leading to the recruitment of autoreactive clonotypes).
- N2) Reducing the number of APCs could also increase competition. We tested models with competition proportional to $1/A$.
- N3) As mentioned, we introduced Z to investigate the competition with subdominant effectors. In Ref. 16, we had only considered monospecific low- and high-avidity T cells.
- N4) The low-avidity pool is largely memory cells, implying that:
- N4a) High-avidity effectors turn over faster than the low-avidity pool (we assumed that $\delta_e \geq \delta_z > \delta_m$).
- N4b) The low-avidity pool proliferates faster than the high-avidity pool (we assumed that $\bar{\alpha}_m > \bar{\alpha}_z \geq \bar{\alpha}_e$). As evidence for this, Fig. 3B shows that the proliferation of splenic 17.6 α /8.3 β (memory) cells is higher than that of the terminally differentiated 17.4 α /8.3 β (effector) CD8⁺ T cells when they are both cultured with NOD splenocytes pulsed with NRP-A7 peptides in IL-2-containing medium (see also Ref. 8).
- N5) High-avidity IGRP_{206–214}-specific CD8⁺ T cells kill β cells more efficiently than do the subdominant effector T cells. That is, for the ratio $\phi = (\text{rate of } \beta \text{ cells killed by } Z)/(\text{rate of } \beta \text{ cells killed by } E)$, we assume that $0 < \phi < 1$.
- N6) Treatment with nanoparticles coated with disease-relevant autoantigenic peptides deletes high-avidity T cells and expands low-avidity T cells corresponding with the given nanoparticle autoantigen, as shown in Fig. 1. Such treatment decreases the average avidity of the total population (17).

- N7) pMHC-nanoparticle treatment can be dose, frequency, and duration dependent. We tested a version of the model with treatment pulses corresponding with the three experimental treatment protocols described earlier.
- N8) Response to treatment varies between individual mice, as shown, for example, in Fig. 7B and 7C. In simulating treatment outcomes, we therefore take into account such heterogeneity as discussed further on.

Facts and assumptions labeled B, E, or N above are model inputs or constraints that the model must satisfy. Based on these, the model equations are

$$\frac{dM}{dt} = \left(\bar{\sigma}_m + \bar{\alpha}_m M \right) A \bar{f}_m \left(P_1 \right) - \delta_m M - \frac{\bar{e}}{A} M \left(M + E + Z \right), \quad (1a)$$

$$\frac{dE}{dt} = \left(\bar{\sigma}_e + \bar{\alpha}_e E \right) A \bar{f}_e \left(P_1 \right) - \delta_e E - \frac{\bar{e}}{A} E \left(M + E + Z \right), \quad (1b)$$

$$\frac{dZ}{dt} = \left(\bar{\sigma}_z + \bar{\alpha}_z Z \right) A \bar{f}_z \left(P_2 \right) - \delta_z Z - \frac{\bar{e}}{A} Z \left(M + E + Z \right). \quad (1c)$$

By E3, reasonable forms for the peptide-dependent T cell proliferation functions $\bar{f}_i(P_j)$ are

$$\bar{f}_i \left(P_1 \right) \equiv \frac{P_1^2}{K_i^2 + P_1^2} \quad \left(i = m, e \right), \quad (1d)$$

$$\bar{f}_z \left(P_2 \right) \equiv \frac{P_2^2}{K_z^2 + P_2^2}, \quad (1e)$$

where K_i represents the level of peptide needed for 1/2-maximal activation of a given clone. By B3, because dominant effector T cells have greater peptide affinity, it is reasonable to take $K_e < K_z < K_m$. The peptide dynamic equations, following E4 and E5, are

$$\frac{dP_1}{dt} = \bar{R}_1 \frac{(E + \phi Z)B}{1 + \mu B} - \delta_{p_1} P_1, \quad (1f)$$

$$\frac{dP_2}{dt} = \bar{R}_2 \frac{(E + \phi Z)B}{1 + \mu B} - \delta_{p_2} P_2. \quad (1g)$$

Here, $(E + \phi Z)B$ is the rate of encounter of effectors and β cells, resulting in β cell death. The parameter μ governs saturation of the β cell killing rate at high β cell levels (16), but we approximate the entire term, $B/(1 + \mu B)$, as a constant by E6.

Based on E7, and incorporating the effect of low-avidity memory CD8⁺ T cells on the suppression of DCs, we take the equation for APCs, A , to be

$$\frac{dA}{dt} = \sigma_a - k_a M A - \delta_a A, \quad (1h)$$

where k_a is a putative suppression rate of APCs per memory cell (which could be zero).

Equations 1a–1h are the basic equations of the model to be explored. According to E4, states with high populations of E and/or Z represent autoimmunity and are henceforth denoted “diseased states,” whereas those with high levels of M and little or no E and Z (or with low levels of all three) are identified with immune quiescence.

We previously considered general forms of T cell production/turnover and showed that models of this class produce qualitative behavior consistent with nanoparticle-treated NOD mouse experiments (16). For example, the fact that the model has to account for both healthy and autoimmune individuals (E8) puts constraints on the types of kinetics. Briefly, the property of bistability is needed (i.e., the model has to support at least two distinct, stable steady states). At the same time, our exploration of many variants of the model assumptions informed our understanding of how kinetic terms affect the model predictions. Our analysis in Ref. 16 indicates that general shapes of the kinetic functions, rather than specific forms, matter to the qualitative behavior. As discussed in Ref. 16, a reduced version of the model explains why treatments aimed at expanding low-avidity cells work much better at the acutely diabetic phase (as observed experimentally in Ref. 17). The same modeling framework also accounts for large cyclic fluctuations in effector cells that can occur in certain cases (10, 16, 22).

Results

Minimal model for T cell competition

We first explored the essential aspects of T cell competition. Based on E6, we reduced Eqs. 1f and 1g using a quasi-steady state assumption, obtaining $P_j \approx R_j(E + \phi Z)$, where R_j is a new constant that includes B, δ_{p_j} , and μ ; see details in the supplementary material. At this first stage, we took the population size of APCs to be constant. Based on E1, we also neglected the comparatively low rates of thymic input ($\sigma_i \approx 0$), which significantly simplifies the analysis without loss of qualitative features (see details in the supplementary material). Then the activation functions \bar{f}_i are directly dependent on the effector cell population $E + \phi Z$ weighted by their β cell killing efficiency; that is,

$$\bar{f}_i(P_j) \approx \bar{f}_i(E + \phi Z) \equiv \frac{(E + \phi Z)^2}{k_i^2 + (E + \phi Z)^2} \quad (i = m, e, z), \quad (2)$$

with $k_m = K_m/R_1$, $k_e = K_e/R_1$, and $k_z = K_z/R_2$. The model 1-2 now depends only on the three variables, M, E, Z . Note that $k_m/k_e = K_m/K_e$ and $k_e/k_z = (K_e/K_z)/(P_1/P_2)$.

To explore the dynamics of this reduced model, we analyzed its three-dimensional phase-space and obtained the following model outputs, labeled R (results) for later reference (more details are provided in the supplementary material):

- R1) There are a number of possible steady-state values, one of which is always a basal background level, at $S_1 = (M_1, E_1, Z_1) = (0, 0, 0)$. This represents nondiabetic NOD mice, or mice that have been treated and recovered from the disease.
- R2) Equilibria with elevated T cell levels representative of autoimmune conditions are those where one or more of the dominant and subdominant effectors, E and Z , are nonzero. Some of these states may also have nonzero values of the protective memory T cells, M .
- R3) Existence, types, and stability of such states depend on values of model parameters. Bifurcation analysis reveals that differences in certain parameter settings are more influential than differences in initial states. In particular, the relative killing efficacy of the dominant and subdominant clones (ϕ) and the avidity ratio k_z/k_e both play key roles in determining the number and properties of steady states (and hence also the overall dynamics).

- R4) Our numerical results suggest that whenever more than one of these equilibria exist, only one is stable.
- R5) Importantly, there is no equilibrium state in which all three types of T cells E, Z, M coexist. That is, one or more clones are always excluded in the competition for sites on APCs.
- R6) The model is robust to variations in values of the parameters α_z, δ_z , and K_z/K_e (i.e., not affected by large parameter uncertainties). In fact, even making these parameters exceed their “biological” ranges does not alter the general behavior of the model significantly.

Treatments expanding memory autoregulatory CD8⁺ T cells

By N6, nanoparticle-based pMHC vaccines lead to expansion of the memory autoregulatory T cell pool (17). We explored how artificially expanding the pool of low-avidity memory cells would affect dynamics and clonal competition. To do so, we initially added a single artificial APC-independent memory cell expansion rate parameter, r_m ; that is, we replaced Eq. 1a by

$$\frac{dM}{dt} = M \left(\bar{\alpha}_m A \bar{f}_m(E + \phi Z) - \delta_m + r_m - \frac{\bar{\epsilon}}{A} [M + E + Z] \right), \quad (1a')$$

as in Ref. 16. We explored the effects of varying r_m in this model (Eqs. 1a', 1b, 1c) using bifurcation analysis (see the supplementary material), with the following results (labeled T for treatment):

- T1) With weak treatment ($0 \leq r_m \leq 1.2 \text{ d}^{-1}$), we usually find effectors (E or Z) with little or no memory cells (M). Beyond some threshold level of r_m , the subdominant effector T cell pool decreases, and memory cell pool simultaneously increases. As r_m increases further, we often see a switch in the dominance from one to another effector class (e.g., Z to E). That is, expansion of the memory autoregulatory cells causes extinction of subdominant clones and takeover by the high-avidity IGRP₂₀₆₋₂₁₄-specific T cell population. This “switch phenomenon” suggests that inappropriate level of treatment can worsen autoimmunity.
- T2) With increasing level of treatment, the healthy state becomes unstable. As in Ref. 16, it is replaced by a new stable steady state with an elevated level of memory autoregulatory cells.

Table I. Values of the standard parameters

Symbol	Meaning	Value	Range
$\sigma_m, \sigma_e, \sigma_z$	APC-dependent thymus inputs ($\sigma_i \approx \bar{\sigma}_i A_d$)	8, 1, 1 cells/d	[5–10], [1–3], [1–3]
$\alpha_m, \alpha_e, \alpha_z$	APC-dependent expansion rates ($\alpha_i \approx \bar{\alpha}_i A_d$)	11, 5.79, 8 d ⁻¹	[10–20], [5–10], [$\alpha_e - \alpha_m$]
$\delta_m, \delta_e, \delta_z$	Turnover rates	0.01, 0.3, 0.1 d ⁻¹	–, –, [$\delta_e - \delta_m$]
$k_m/k_e, k_z/k_e$	M -to- E, Z -to- E avidity ratios	10, 5	[6–9], [2– k_m/k_e]
ϵ	Competition parameter ($\epsilon \approx \bar{\epsilon}/A_d$)	5.23×10^{-6} (cell \times d) ⁻¹	[5–10] $\times 10^{-6}$
δ_a	Turnover rate of APCs	0.3 d ⁻¹	[0.24–0.46]
σ_a	Influx of APCs from bone marrow	3×10^5 cell/d	[3–4] $\times 10^5$
k_a	Rate of APC suppression	8.5×10^{-6} (cell \times d) ⁻¹	[8–9] $\times 10^{-6}$
A_d	No. of APCs at autoimmune state	4×10^5 cells	
r_m^*, r_e^*	M, E expansion, deletion rates	0.2, 0.1 ($\mu\text{g} \times \text{d}$) ⁻¹	[0.1–0.65], [0.05–0.15]
δ_{N_p}	Degradation rate of pMHC-nanoparticles	0.06 d ⁻¹	[0.06–0.36]
d	pMHC-nanoparticle injection dose	7.5, 7.5/5, 7.5/20 μg	
w	pMHC-nanoparticle injection duration	0.5 min	
Φ	Relative killing efficacy of Z -to- E		[0–1]

The notation [a-b] indicates the lower, a, and upper, b, values used for the range of values of a given parameter.

- T3) If the relative killing efficacy is $\phi \sim 0.3$, both types of effectors (E and Z) grow, and memory cells are suppressed (i.e., this is the worst-case scenario in terms of damage to β cells; see the supplementary material for details). This could explain the class of NOD mice that are not responsive to treatment and remain hyperglycemic.
- T4) When $\phi \sim 1$, effectors E are driven to extinction, whereas M and Z populations remain. Although this behavior is similar to case T1, it represents a limiting case, where the killing efficacy of dominant (E) and subdominant (Z) effector T cells is the same, and its resultant outcome on β cell killing would be practically indistinguishable.
- T5) When the avidity ratio is $k_z/k_e \sim 9$, Z goes extinct whereas M and E remain. The behavior is then the same as the M, E model analyzed in Ref. 16, so we omit details. Briefly, the diseased state consists of M and E (with $Z \approx 0$), and effectors E decrease as treatment r_m increases. After a 4-fold increase in the value of r_m , this state disappears (in a saddle node bifurcation). Thence, the healthy steady state is stable. This case could represent the class of NOD mice that have been successfully treated.

Expansion of M and deletion of E

We next asked how predictions change if nanoparticles also kill IGRP₂₀₆₋₂₁₄-specific effector cells in addition to expanding memory T cells. We modified the model to include both effects. Further, to prepare for our investigation of injection, dose, and treatment frequency protocols, we also track the turnover of circulating pMHC-nanoparticles, N_p . We rescale the variables, setting $M = k_e m$, $E = k_e e$, and $Z = k_e z$ (see details in the supplementary material) to obtain

$$\frac{dm}{dt} = m (\alpha_m f_m(e + \phi z) - \delta_m - \varepsilon^* [m + e + z] + r_m^* N_p), \quad (3a)$$

$$\frac{de}{dt} = e (\alpha_e f_e(e + \phi z) - \delta_e - \varepsilon^* [m + e + z] - r_e^* N_p), \quad (3b)$$

$$\frac{dz}{dt} = z (\alpha_z f_z(e + \phi z) - \delta_z - \varepsilon^* [m + e + z]), \quad (3c)$$

$$\frac{dN_p}{dt} = I(t) - \delta_{N_p} N_p. \quad (3d)$$

Here, $f_i = (e + \phi z)^2 / ([k_i/k_e^2] + [e + \phi z]^2)$, $i = m, e, z$, $r_m \approx r_m^* N_p$, and $r_e \approx r_e^* N_p$. $I(t)$ is a function that represents the frequency and dose of injections of pMHC-laden nanoparticles, and δ_{N_p} is their decay rate. The three parameters r_m^* , r_e^* , δ_{N_p} are unknown. Hence, we consider estimates of relevant parameters before analyzing the new model variant.

Parameter estimation

We briefly explain how parameters were estimated for our simulations of the model with treatment protocols (see further details in the supplementary material and in Refs. 15, 16, 19, 22).

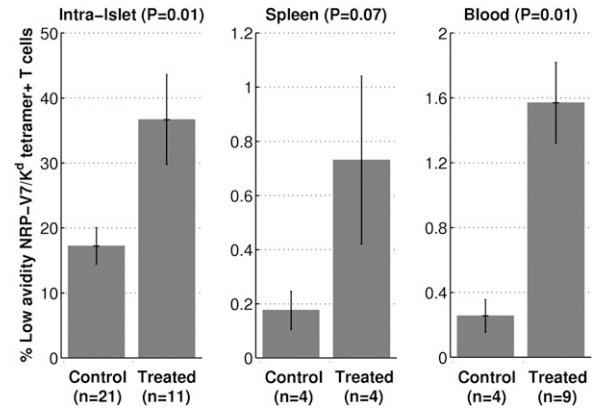


FIGURE 1. Bar graphs showing the experimentally measured average expansion of low-avidity NRP-V7/K^d-specific CD8⁺ T cell pool in islets, spleen, and circulating blood in NOD mice. By comparison with control mice, treated mice exhibit ~2- to 6-fold increase in the size of this population. Protocol 1 was followed in each experiment (n, number of mice used; mean \pm SEM values from n mice per study).

Parameters for T cell dynamics. As in Refs. 15 and 22, rates of turnover of dominant effector and memory T cells (δ_e , δ_m) and typical T cell counts in health and in autoimmunity were used to find appropriate ranges for the maximal rates of proliferation α_i . Because the level of native autoantigen is not easily measurable, it is difficult to assign absolute levels to parameters K_i . We used the relative avidities of clones to provide a relative peptide effect. The rescaling introduced earlier effectively replaces the parameters k_m , k_e , and k_z by their ratios, $k_m/k_e (= K_m/K_e)$ and k_z/k_e . The variables m , e , z , become dimensionless in this case (see details in the supplementary material). A summary of the estimated values of the standard and scaled parameters are given in Table I and Table II, respectively.

Treatment parameters and mouse heterogeneity. The half-life of circulating unconjugated nanoparticles is 10 h (decay rate $\delta_{N_p} \approx 1.66 \text{ d}^{-1}$), but the rate of turnover of pMHC-nanoparticles in islets is unknown. We must estimate the treatment-dependent parameters for rates of expansion, deletion, and nanoparticle turnover rate (r_m^* , r_e^* , and δ_{N_p}) to simulate our model with treatment protocols. Paucity of data points makes it impossible to apply direct curve-fitting to estimate these three parameters, so we used an indirect approach.

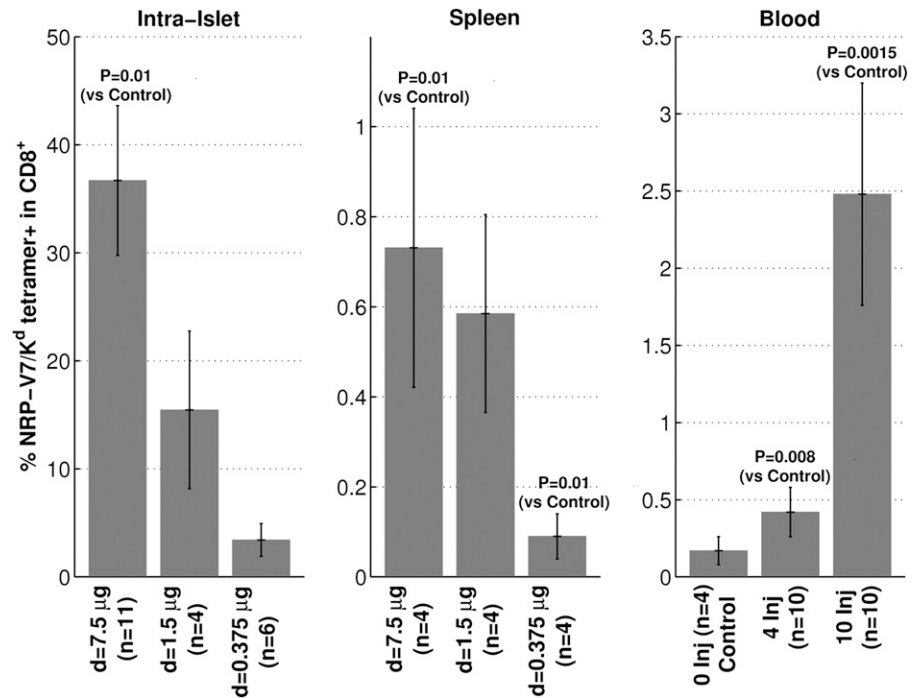
We simulated clonal dynamics using Eq. 3 in 25 individual model “mice” whose parameter values were randomly drawn from uniform distributions in ranges shown in Table I. In each case, arbitrary initial conditions were also assumed. These random choices represent interindividual differences and variability, see N8, but note also E8. At each time point, the percentage of memory cells in each “mouse” j was calculated, $\{100 m_j(t) / (m_j(t) + e_j(t) + z_j(t))\}$, and averaged over $n = 25$ simulated “mice.” Results were compared with experimental observations of Ref. 17 that are summarized in Figs. 1 and 2.

Fig. 3 shows that the APC-dependent expansion of memory cells is bigger than effector cells. As for the nanoparticle-dependent expansion, we first considered the case that pMHC-nanoparticles only expand the memory cell pool (i.e., $r_e^* = 0$, $r_m^* > 0$). The

Table II. Default values of the scaled parameters

Symbol	Value	Symbol	Value	Symbol	Value	Symbol	Value
σ_m^*	8×10^{-5}	σ_e^*	10^{-5}	σ_z^*	10^{-5}	ε^*	0.523
α_m^*	2.75	α_e^*	1.45	α_z^*	2	$\bar{\varepsilon}^*$	0.2092

FIGURE 2. The average expansion of low-avidity NRP-V7/K^d-specific CD8⁺ T cell pool is dose and frequency dependent in NOD mice. Applying protocol 1 at increasing doses ($d = 0.375, 1.5, 7.5 \mu\text{g}$) leads to a gradual increase in the average size of this population in islets and spleen. Similarly, applying protocols 2 and 3 leads to a gradual increase in the average size of the memory T cell pool in the circulating blood (mean \pm SEM values from n mice per study).



model (based on Fig. 4) was run initially three times with pre-treatment conditions, leading to average percentages of memory cells of 18.17, 11.03, and 10.2%, respectively, close to the experimental average of 17.24% obtained in Ref. 17. We then implemented discrete injection “treatments” using short (square-wave) pulses for the input $I(t)$ in Eq. 3d (see earlier text and the supplementary material). Results of standard treatment (protocol 1) at full dose are shown in Fig. 5.

We used Fig. 5 to find parameter regimes in the $\delta_{N_p} r_m^*$ -plane that lead to an expansion of memory cells in the range 33–38%, close to the experimentally observed $\sim 36.69\%$ level (see Fig. 1). The parameter regimes producing appropriate results are shown in white. Black denotes inappropriate parameter choices. Similar

conclusions were found at lower doses (details in the supplementary material). Further, we found that shorter nanoparticle half-life (for r_m^* fixed at a low value) results in greater average percentage of memory cells (Supplemental Material). Investigating the individual “mice” that make up this simulated group, however, we found that many became and remained diabetic. Treatment failed to move their states from the basin of attraction of autoimmunity to the basin of attraction of the healthy state; after each injection, they still progressed toward the autoimmune state. We observed that at high rates of turnover of the nanoparticles (large δ_{N_p} values), the treatment was insufficient for appropriate accumulation of memory cells.

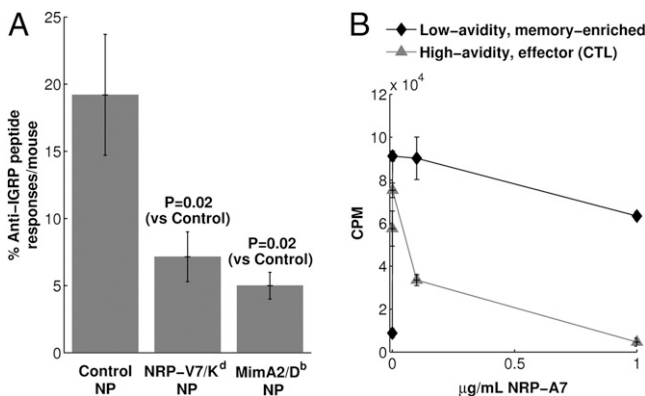


FIGURE 3. APC-dependent expansion of effector and memory IGRP-specific CD8⁺ T cells. *A*, Percentages of islet-associated CD8⁺ T cells (obtained from control-nanoparticle-treated [$n = 9$], NRP-V7/K^d-nanoparticle-treated [$n = 5$], and MimA2/D^p-nanoparticle-treated [$n = 4$] NOD mice) that elicited positive responses when cocultured with splenocytes pulsed with each of the 76 IGRP epitopes. *B*, Low-avidity 17.6-TCR-transgenic splenic effector T cells (black line) proliferate more efficiently than the 17.4-TCR-transgenic splenic T cells (gray line) when both are cultured with NOD splenocytes pulsed with NRP-A7 peptides in IL-2-containing medium. CPM, counts per minute (mean \pm SEM values from n mice or cultures per study).

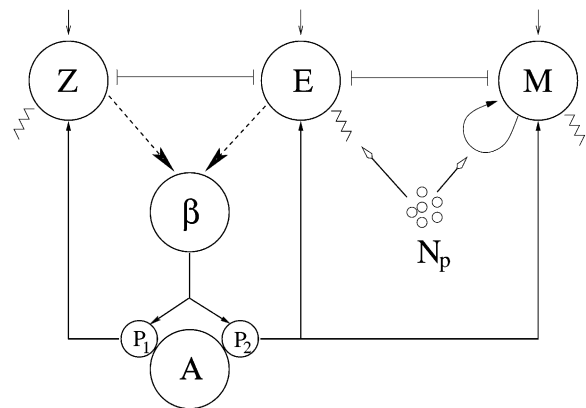


FIGURE 4. Schematic diagram of the model showing IGRP_{206–214}-specific low-avidity (M), high-avidity (E), and other autoreactive non-IGRP_{206–214}-specific CD8⁺ T cells (Z). Thymic input of naive cells (thin vertical arrows) are small compared with other influences. T cell pools compete (thin horizontal lines); inhibition between M and Z is also present (arrow not shown). Effectors E and Z kill β cells (dashed lines with large arrows) producing two types of autoantigens: P_1 (representing IGRP_{206–214}) and P_2 (autoantigens corresponding with all other subdominant specificities). Peptide-laden APCs (A) cause activation of E and M by peptide P_1 and of Z by peptide P_2 . Treatment by nanoparticles, N_p , expands memory cells at rate r_m and possibly increases turnover of effectors E (zigzag line) by rate r_e .

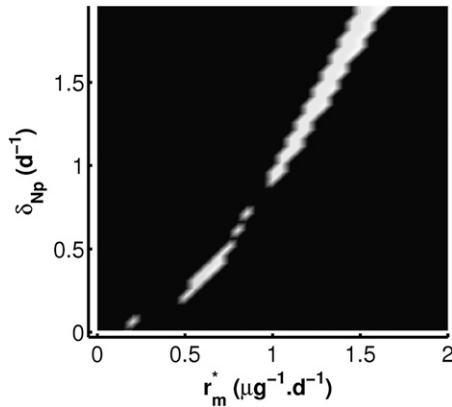


FIGURE 5. Average percentage of memory cells in 25 simulated “mice” is calculated for increasing values of δ_{N_p} in the range $0\text{--}2\text{ d}^{-1}$ and r_m^* in the range $0\text{--}2\text{ }(\mu\text{g d}^{-1})$ (with $r_e^* = 0$), after applying protocol 1 at the injection dose $d = 7.5\text{ }\mu\text{g}$. For each “mouse,” other parameters were selected randomly from ranges listed in Table I using uniform distributions. The white regions represent the parameter regimes for δ_{N_p} and r_m^* that produce average percentages of memory cells within the experimentally observed range of 33–38%. Black regions correspond with parameters that produce percentages outside the range.

We next included the direct deletion of dominant effector T cell clone by the pMHC-nanoparticles ($r_e^* \neq 0$). We simulated 25 “mice” with $0 \leq r_e^* \leq 2\text{ }(\mu\text{g}\cdot\text{d})^{-1}$ taking δ_{N_p} and r_m^* from the white regions of Fig. 5. We excluded parameter values that led to reductions in the average percentage of memory cells as inconsistent with experimental observations. We repeated a similar procedure using protocols 2 and 3 and data in Fig. 2 to exclude inappropriate parameter ranges. Our results (data not shown) reveal that the appropriate ranges of the parameters are $0.06 \leq \delta_{N_p} \leq 0.36\text{ d}^{-1}$, $0.1 \leq r_m^* \leq 0.65\text{ }(\mu\text{g}\cdot\text{d})^{-1}$, and $0.05 \leq r_e^* \leq 0.15\text{ }(\mu\text{g}\cdot\text{d})^{-1}$. We found that nanoparticle decay rate δ_{N_p} should be much lower than the value $\tilde{\delta}_{N_p}$ for unconjugated nanoparticles. This finding is consistent with our earlier observation about the effect of $\tilde{\delta}_{N_p}$ values. In fact, for $\delta_{N_p} \sim \tilde{\delta}_{N_p}$, we found that more than 90% of “mice” that respond to treatment do so after a single injection, a feature that is never observed experimentally.

Model response to the standard treatment (protocol 1)

With the above parameter estimates, we next simulated a heterogeneous population of 100 model “mice” satisfying Eqs. 3a–3d (with random initial conditions and parameters described above) by using protocol 1. The treatment parameters were chosen to be $\delta_{N_p} = 0.06\text{ d}^{-1}$, $r_m^* = 0.2\text{ }(\mu\text{g d}^{-1})$, and $r_e^* = 0.1\text{ }(\mu\text{g d}^{-1})$. Fig. 6 shows a representative sample of time series for the memory (solid), dominant effector (dashed), and subdominant effector (dotted) T cell pools.

Fig. 6A is a typical example of complete recovery. The actual route to recovery varies (4, 5, and 8% of the “mice” recover after the first, second, or third injection, respectively). Fig. 6A exhibits the switch phenomenon: the dominant effectors are replaced by subdominant effectors (Z replaces E), after which Z is also extinguished. A similar switching behavior occurs in Fig. 6E, where no recovery takes place. However, Fig. 6B and 6C shows “mice” that remain diabetic but display significant to moderate improvements, respectively: in Fig. 6B, Z is suppressed, and in Fig. 6C, there is a reduction in the population of E . Finally, Fig. 6D shows a case where there is hardly any response and where an elevated level of the subdominant effectors occurs. These distinct possibilities illustrate the diversity of outcomes.

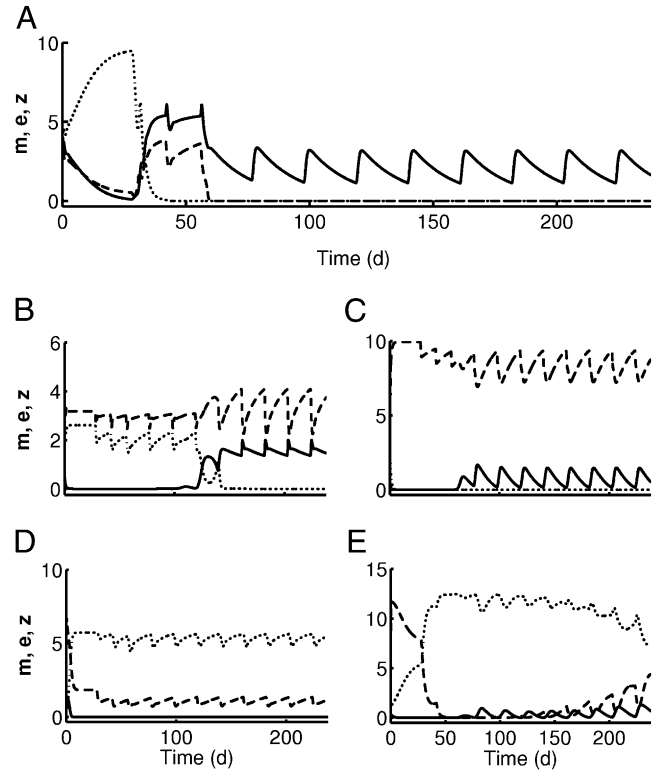
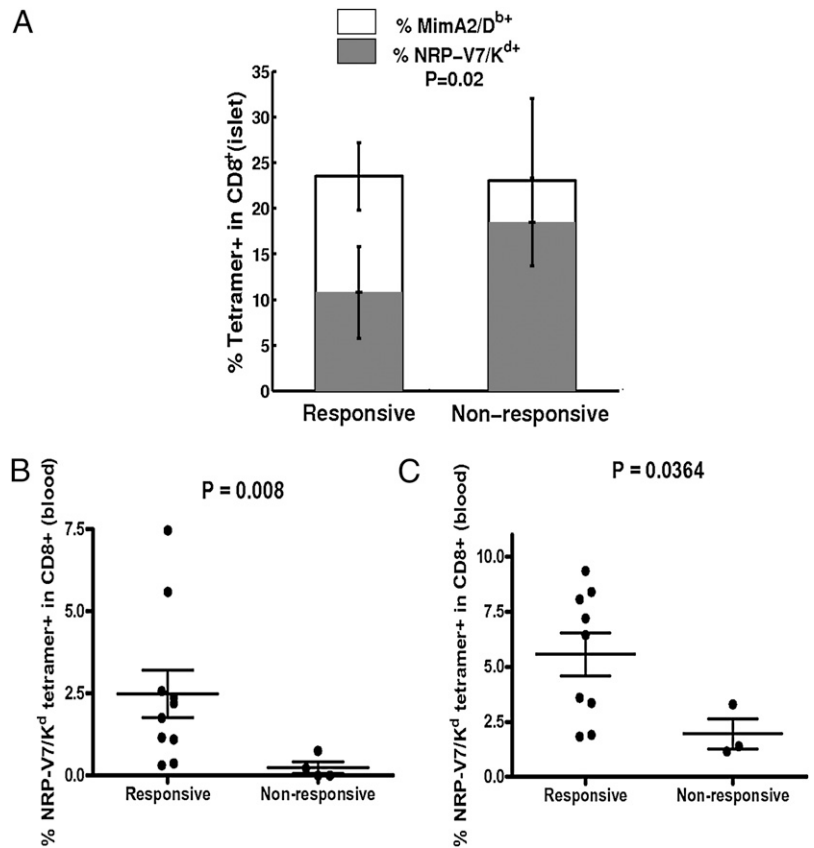


FIGURE 6. A representative sample of T cell time series in five typical cases from a set of 100 simulated “mice” (Eqs. 3a–3d with protocol 1, $\delta_{N_p} = 0.06\text{ d}^{-1}$, $r_m^* = 0.2\text{ }[\mu\text{g}\cdot\text{d}]^{-1}$, and $r_e^* = 0.1\text{ }[\mu\text{g}\cdot\text{d}]^{-1}$). Each panel shows (in scaled form) the levels of low-avidity memory cells m (solid line), high-avidity dominant e (dashed line), and subdominant effector cells z (dotted line). The average percentage of memory cells increases from 12.7% before treatment to 32.3% after treatment, close to experimentally observed levels. The profile shown in A represents a “mouse” cured after at most three injections; B and C represent significant ($0 \leq Q \leq 0.7$) and moderate ($0.7 \leq Q \leq 1$) improvement, respectively; whereas D and E display no improvement ($Q = 1$). Here, $Q = (e_j[t_{\text{after}}] + z_j[t_{\text{after}}]) / (e_j[t_{\text{before}}] + z_j[t_{\text{before}}])$, where $t_{\text{after}} = 238\text{ d}$. A subset of such cases exhibits the switch phenomenon shown in E.

We can understand the reasons for such disparities in Fig. 6 as follows. For a given model “mouse,” the existence of various equilibria, their stability, and their basins of attraction depend on parameters and initial conditions that differ slightly between individuals, reflecting the physiological variability between mice. Variability in immunological history may also affect the individual’s initial immune makeup (as represented by random initial conditions). In a given “mouse,” initial conditions that fall in the region of state space attracted to the autoimmune state will evolve to full-blown autoimmunity (high E and/or Z), whereas those in the (much smaller) basin of attraction of the healthy state will remain diabetes free (low E and Z , possibly high M). Treatment changes the configuration of these basins for the duration of the therapeutic effect. States previously in one basin of attraction may now be in another. In this way, autoimmune “mice” can be “cured” provided their evolution toward the healthy state is “fast enough” relative to the timescale over which the treatment is effective. If the nanoparticle half-life and therapeutic potential is long enough, and the immune state re-equilibrates quickly enough, it can approach the healthy state and stay in its basin of attraction. Once those particles are cleared, however, the state space returns to the pretreatment configuration, so some “mice” may still be too far from the healthy state to be cured. Detailed discussion of such theoretical reasoning is given in Ref. 16.

FIGURE 7. Targeting one epitope-specific clone using pMHC-nanoparticle therapy leads to the expansion and dominance of other pathogenic clones in non-responsive (diseased) NOD mice. Percentages of tetramer + CD8⁺ T cells in NOD mice treated (using protocol 1) with (A) MimA2/D^b nanoparticles (islets) or with (B, C) NRP-V7/K^d nanoparticles (blood). Four-week-old mice that did not respond to treatment (*n* = 3) in A expressed reduced level of MimA2-reactive T cells and elevated level of NRP-V7-reactive T cells in their islets compared with those of the same-age group mice that responded to treatment (*n* = 10). Similar outcomes were obtained in (B) 10-wk-old and (C) acutely diabetic mice treated with NRP-V7/K^d nanoparticles (here, responsive mice expressed elevated level of NRP-V7-reactive T cells, in contrast with nonresponsive mice) (mean ± SEM values from *n* mice per study).



To test predictions of the model, we quantified the relative proportions of T cells in memory versus effector classes in a group of 4-wk-old NOD mice treated with pMHC-nanoparticles coated

with MimA2/D^b using protocol 1. Recall that such treatment is aimed at expanding the low-avidity protective T cell pool within the MimA2/D^b-specific clone at the expense of its high-avidity counterpart. We measured the relative levels of MimA2/D^b-specific T cells (predominately low-avidity memory T cells due to pMHC-nanoparticle treatment) and the level of NRP-V7/K^d-specific T cells (predominately effectors) in islets in each mouse and classified the mice as responsive versus nonresponsive (i.e., diseased) after treatment. Results are shown in Fig. 7A. In agreement with model assumptions, treatment led to the presence (and/or expansion) of the protective low-avidity MimA2/D^b-

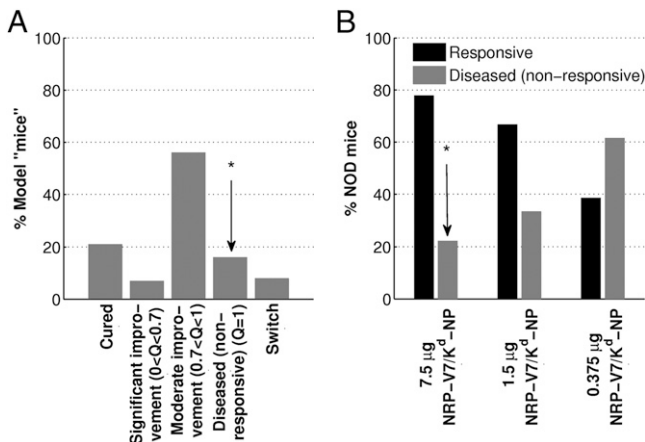


FIGURE 8. Treatment responses in model “mice” and in NOD mice. A, Relative frequencies of the five outcomes shown in Fig. 6: cured after at most three injections (21%), diseased with significant improvement in the level of low-avidity T cells, $0 \leq Q \leq 0.7$ (7%), diseased with modest improvement in the level of low-avidity T cells, $0.7 \leq Q \leq 1$ (56%), diseased not responding to treatment, $Q = 1$ (16%), and diseased, exhibiting the switch phenomenon (8%). *Q* is as defined in Fig. 6. B, The incidence of diabetes increased with decreasing NRP-V7/K^d-nanoparticle dose. Black columns represent NOD mice that responded to treatment, and gray columns represent mice that did not respond and became hyperglycemic ($p = 0.0532$ for 7.5 µg dose versus 1.6 µg dose, and $p = 0.0538$ for 7.5 µg dose versus 0.375 µg dose; mean ± SEM values from *n* mice per study). The nonresponsive (diseased) group in both A and B (highlighted by an asterisk) are comparable (16% versus 23%, respectively), confirming the model prediction.

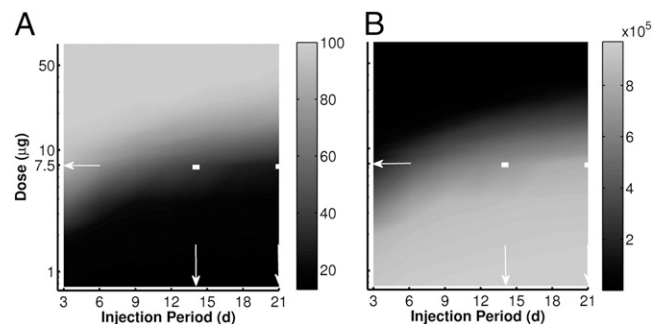


FIGURE 9. The influence of injection dose and period on treatment outcomes in 100 simulated “mice” for a given treatment protocol. Treatment parameters are the same as in Fig. 6. A, The average percentage of memory cells, ranging from ~13% (black) to 100% (white). B, The average sum of effectors (*E* + *Z*), ranging from 0 cells (black) to ~10⁶ cells (white). Arrows denote dose and frequency of the two phases of protocol 1. The solid white rectangle (corresponding with the biweekly injections of 7.5 µg pMHC-nanoparticles) is at the border between effective and non-effective treatment regimens.

specific T cells in all mice. In agreement with model predictions, nonresponsive mice had a far greater proportion of the dangerous high-avidity NRP-V7/K^d-specific T cells (not targeted by the pMHC-nanoparticle treatment and, in most cases, largely an effector T cell population). Islets were infiltrated in the latter case by other autoantigen-specific T cells from those targeted by pMHC-nanoparticles coated with MimA2/D^b. Such behavior is indicative of the switch phenomenon described by our model whereby targeting a T cell clone with a given specificity may lead to the dominance (and islet infiltration) by other epitope-specific T cells that are predominately effectors.

Applying the same treatment protocol to 10-wk-old mice (Fig. 7B) and to acutely diabetic mice (Fig. 7C), using this time pMHC-nanoparticles coated with NRP-V7/K^d, resulted in similar outcomes; that is, observing in both groups of mice significant elevation in the size of memory NRP-V7/K^d-specific T cells in the responsive NOD mice compared with that in nonresponsive mice (due presumably to the dominance of other epitope-specific effector T cells not targeted by the pMHC-nanoparticle treatment).

To compare predicted treatment outcomes with those observed experimentally, we classified our 100 simulated runs (protocol 1) into responsiveness classes shown in Fig. 8A. We found ~21% recovery, 7% significant and 56% modest improvement, and 16% no improvement. Improvement in an individual was defined as decrease in the level of effectors [$e + z$] subsequent to treatment. We assessed this ratio, Q , (see caption, Fig. 6) at $t = 238$ d, at the time that measurements were taken in the experiment (2 wk after the last injection). We next compared these predictions with experimental treatment results, shown in Fig. 8B. The predicted frequency (16%) of model “mice” not responding to treatment (identified by an asterisk in Fig. 8A) is consistent with the incidence of diabetes (~23%) obtained experimentally from ($n = 11$) 4-wk NOD mice treated with 7.5 μ g NRP-V7/K^d nanoparticles using protocol 1 (identified by an asterisk in Fig. 8B). Decreasing the dose of injection by 5- and 20-fold increased the incidence of diabetes in both groups, especially the latter, in accordance with what we have observed in Fig. 2.

Optimizing treatment strategy

We asked whether treatment protocols could be optimized using our model. We considered multiple protocols in which both dose and frequency of injections were adjusted in a series of “in silico” experiments with a population of 100 “mice” as follows.

We varied the period between injections (from 3 to 21 d) and the dose of nanoparticles (from 0 to 50 μ g). In Fig. 9, we show both the average percentage of memory cells (M , Fig. 9A) and the sum of the dominant and subdominant effector T cell populations ($E + Z$, Fig. 9B) on a relative logarithmic scale. In both panels of Fig. 9, white (black) colors represent higher (lower) T cell populations (thus, healthy outcomes are at *top left*, with high M , low E and Z , and severe autoimmunity is at *bottom right*, with low M , high E and Z). On the figure, arrows point to the dose and period of the standard treatment (initial phase, biweekly injections with a dose of 7.5 μ g). The white rectangle corresponds with outcome of the standard treatment, clearly observed to be at the border between effective and noneffective regimens. A second rectangle at the same dose corresponding with the second phase of the same protocol (i.e., at a 3-wk period) lies outside the effective treatment regimen.

Observe the logarithmic vertical scale in Fig. 9A and 9B: it is more difficult to optimize treatment by increasing the dose (moving vertically on these diagrams). For a fixed period (e.g., 3 wk), the dose has to be tripled to obtain a reasonable outcome. Slightly raising the dose (e.g., to 10 μ g) and decreasing the injection period (e.g., from 2 wk to 9 d) achieves a much better result. Fig. 9A and 9B also explain why simulated “mice” that respond to treatment do so within the first three injections at 2 wk apart. Continued treatment at this period is essential for good prognosis. If the injection period is increased to 3 wk, the treatment ceases to be effective, and autoimmunity returns.

We compared our predictions associated with dose and frequency with the experimental results obtained from NOD mice treated with NRP-V7/K^d nanoparticles following three different treatment schedules: protocol 1 at various doses (7.5, 1.5, and 0.375 μ g); protocol 4 and protocol 5 at a dose of 7.5 μ g. Fig. 10A

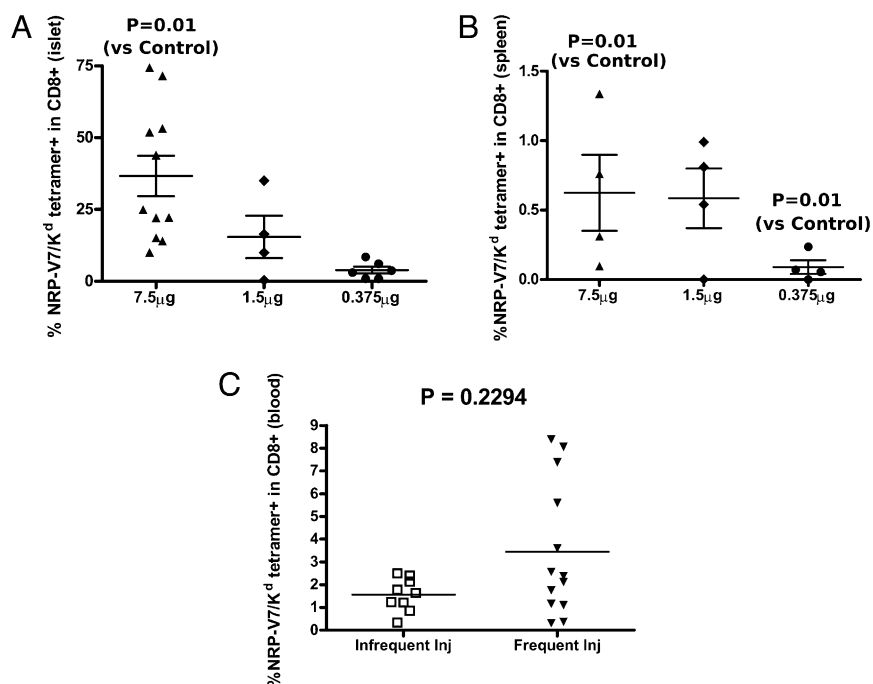


FIGURE 10. The expansion of low-avidity NRP-V7/K^d-specific memory T cells depends on dose and frequency of NRP-V7/K^d-nanoparticle injections. The percentage of NRP-V7/K^d tetramer + CD8⁺ T cells in islets (A), spleen (B), and blood (C) are shown. Increasing the dose from 0.375 to 1.5 and 7.5 μ g (A, B) increased the percentage of memory cells in islets and spleen. Similarly, increasing the frequency 5-fold (from 1 injection/2.5 wk to 2 injections/wk) in C also increased the percentage of memory cells in the blood. A comparison of data from spleen and blood indicates that the increase in frequency was more effective than the increase in dose (mean \pm SEM values from n mice per study).

and 10B shows the relative sizes of the predominately memory NRP-V7/K^d-specific T cells in islets and in the spleen, respectively, after treatment using protocol 1. The outcomes here confirm that the dependence of relative sizes of memory cell pools on the dose is nonlinear: increasing the dose becomes less and less efficient at expanding *M* and suppressing other clones (note the log dose scale in Fig. 9A and 9B). We observe a more dramatic increase in the average pool sizes of NRP-V7/K^d-specific T cells when the dose was initially increased 4-fold (from 0.375 to 1.5 μg) than when the dose was increased 5-fold (from 1.5 to 7.5 μg).

Furthermore, Fig. 10C suggests that increasing the injection frequency produced better results than increasing the dose. In fact, increasing the frequency of injection from once per 2–3 wk (protocol 5) to twice per week (protocol 4) (i.e., a 5-fold increase) increased the level of low-avidity NRP-V7/K^d-specific T cells by a factor of 2.2, whereas a similar increase in the dose produced only a factor of 1.2 increase (Fig. 10B). Data were currently available for spleen and blood. These experimental observations are consistent with our model predictions in Fig. 9.

Model variants

We asked whether results of the model could be due to artifacts associated with our simplification of the process. We therefore ran further tests of related model variants. First, we included thymic input ($\sigma_m \sim 8 \text{ cells d}^{-1}$ and $\sigma_e, \sigma_z \sim 1 \text{ cell d}^{-1}$) (15) to ascertain whether omitting this affects the conclusions. We obtained qualitatively and quantitatively similar results (data not shown) that were at most 1% different from those described here, even when σ_i were altered significantly.

Next, we examined the possible effect of low-avidity IGRP_{206–214}-specific CD8⁺ T cells on APCs by investigating a hypothesis suggested in Ref. 17 and explored in Ref. 16 that these T cells also suppress APCs. We explored model variants that explicitly included this effect. Briefly, we simulated the standard model but included Eq. 1h, where mortality or suppression of APCs stems from interactions with clone *M*. We simulated a heterogeneous population of 500 “mice” and followed their pools of T cells and APCs (see details in the supplementary material). We compared the results with those generated by system 3a–3d. The recorded responses were almost always identical to those observed previously. The interactions of the various T cell pools remained the same, and the relative frequencies of the five standard outcomes shown in Fig. 8 were very similar. The indirect effects of this pMHC-nanoparticle therapy on non-IGRP_{206–214}-specific CD8⁺ T cells (*Z* pool) were also very similar.

Discussion

In this paper, we considered the interactions of IGRP_{206–214}-specific low-avidity memory autoregulatory CD8⁺ T cells with their high-avidity counterparts and another pool representing all other CD8⁺ T cell specificities implicated in T1D. To do so, we adapted a modeling framework developed by repeated cycles of experiment and modeling in our group over the past decade. In this study, we used this quantitative framework to investigate treatment by pMHC-nanoparticles that expand the regulatory pool at the expense of other clones.

Analysis of the minimal model variant (see the section *Minimal model for T cell competition*) is concordant with the experimental observation that both healthy and diseased outcomes are observed (results R1–R3) and that one or another specificity can evolve to dominate the response (R3–R5). Variations between individual animals (affecting parameter values) as well as immunological experience (affecting the initial state of each animal) were also shown to affect the prognosis of health or disease in absence of

treatment (R6, R7). A second model variant that incorporates treatments that expand low-avidity CD8⁺ T cells (using the expansion parameter r_m in Eq. 1a') recapitulates the observations that monoclonal nanoparticles coated with disease-relevant pMHC can blunt T1D in NOD mice by increasing the dominance of autoregulatory memory-like peptide-specific CD8⁺ T cells (T1, T2). Importantly, we showed that suppressing the recruitment of dominant effectors by cognate pMHC nanovaccines can potentially allow for the expansion of the subdominant, noncognate effectors (T3), in support of hypotheses put forward in Ref. 17. We found cases in which mere expansion of the autoregulatory specificities resulted in the switch between effectors from dominant to subdominant (or vice versa) (T3, T4). This demonstrates the importance of finding treatments that can dampen all effector populations (e.g., by targeting APCs).

The model is focused on a subset of cells within a highly complex immunological system and hence has obvious limitations. For example, we did not explicitly model all stages involved in the recruitment of these islet-specific T cells, eventual formation of tertiary lymphoid structures (processes that are on different timescales), or recruitment of non-islet-specific T cells (23), likely to have a minor effect on predictions. We also did not consider the effect of declining β cell population (a feature of our previous work) (16). We lumped many subdominant T cell specificities to islet autoantigens into a single pool (represented by *Z*), whereas in reality, these consist of a heterogeneous collection of competing clones, Z_1, Z_2, \dots, Z_n . Nevertheless, our model captures essential features of clonal competition, demonstrating how provoking the expansion of one clone can affect the expansion and intra-islet accumulation of other clones.

To overcome the challenge of finding parameter ranges typical of a heterogeneous population of mice, we simulated many individuals using a wide range of parameters and averaged the results, as done experimentally when samples for multiple mice are pooled for T cell measurements. This facilitated direct comparison of model and experiment. We found that the ratio of killing ability of the subdominant and dominant effectors, represented by ϕ , and the ratio of avidities k_z/k_e affect T cell population equilibria. This suggests that the diversity in T cell population sizes measured for NOD mice (17) may be due to the variation in the level of avidity and the killing efficacy of the surviving clones that escape peripheral and central tolerance in each mouse. It is important to take this diversity into account in considering treatment options.

As shown in experiments suggested by the model, there is broad agreement in qualitative and quantitative observations. Using the tested model, we could then explore optimization of treatment strategies with respect to dose and frequency of injections. We identify regimens where treatment is expected to be ineffective, moderate, or effective. In our most significant finding, we predict that lowering the period between injections provides a greater benefit than does increasing the treatment dose (given the estimated treatment parameters). A strategy for future consideration is increasing the half-life of the nanoparticles to increase the effectiveness of each injection. We also noted that the standard treatment (protocol 1) is effective in its first three injections only, becoming ineffective once the injection period is decreased to one per 3 wk. In short, our model suggests how treatment could be more strategically designed. We recommend that once a standard protocol is initiated, the response of T cells should be determined. With that response, one can adjust the protocol (e.g., increase frequency of injection or dose) to optimize the prognosis.

Disclosures

The authors have no financial conflicts of interest.

References

- Lieberman, S. M., T. Takaki, B. Han, P. Santamaria, D. V. Serreze, and T. P. DiLorenzo. 2004. Individual nonobese diabetic mice exhibit unique patterns of CD8⁺ T cell reactivity to three islet antigens, including the newly identified widely expressed dystrophin myotonia kinase. *J. Immunol.* 173: 6727–6734.
- Amrani, A., P. Serra, J. Yamanouchi, J. D. Trudeau, R. Tan, J. F. Elliott, and P. Santamaria. 2001. Expansion of the antigenic repertoire of a single T cell receptor upon T cell activation. *J. Immunol.* 167: 655–666.
- Anderson, B., B.-J. Park, J. Verdager, A. Amrani, and P. Santamaria. 1999. Prevalent CD8⁺ T cell response against one peptide/MHC complex in autoimmune diabetes. *Proc. Natl. Acad. Sci. USA* 96: 9311–9316.
- DiLorenzo, T. P., R. T. Graser, T. Ono, G. J. Christianson, H. D. Chapman, D. C. Roopenian, S. G. Nathenson, and D. V. Serreze. 1998. Major histocompatibility complex class I-restricted T cells are required for all but the end stages of diabetes development in nonobese diabetic mice and use a prevalent T cell receptor α chain gene rearrangement. *Proc. Natl. Acad. Sci. USA* 95: 12538–12543.
- Santamaria, P., T. Utsugi, B.-J. Park, N. Averill, S. Kawazu, and J.-W. Yoon. 1995. Beta-cell-cytotoxic CD8⁺ T cells from nonobese diabetic mice use highly homologous T cell receptor alpha-chain CDR3 sequences. *J. Immunol.* 154: 2494–2503.
- Verdager, J., D. Schmidt, A. Amrani, B. Anderson, N. Averill, and P. Santamaria. 1997. Spontaneous autoimmune diabetes in monoclonal T cell nonobese diabetic mice. *J. Exp. Med.* 186: 1663–1676.
- Verdager, J., J.-W. Yoon, B. Anderson, N. Averill, T. Utsugi, B.-J. Park, and P. Santamaria. 1996. Acceleration of spontaneous diabetes in TCR-beta-transgenic nonobese diabetic mice by beta-cell cytotoxic CD8⁺ T cells expressing identical endogenous TCR- α chains. *J. Immunol.* 157: 4726–4735.
- Han, B., P. Serra, J. Yamanouchi, A. Amrani, J. F. Elliott, P. Dickie, T. P. DiLorenzo, and P. Santamaria. 2005. Developmental control of CD8 T cell-avidity maturation in autoimmune diabetes. *J. Clin. Invest.* 115: 1879–1887.
- Lieberman, S. M., A. M. Evans, B. Han, T. Takaki, Y. Vinnitskaya, J. A. Caldwell, D. V. Serreze, J. Shabanowitz, D. F. Hunt, S. G. Nathenson, et al. 2003. Identification of the beta cell antigen targeted by a prevalent population of pathogenic CD8⁺ T cells in autoimmune diabetes. *Proc. Natl. Acad. Sci. USA* 100: 8384–8388.
- Trudeau, J. D., C. Kelly-Smith, C. B. Verchere, J. F. Elliott, J. P. Dutz, D. T. Finegood, P. Santamaria, and R. Tan. 2003. Prediction of spontaneous autoimmune diabetes in NOD mice by quantification of autoreactive T cells in peripheral blood. *J. Clin. Invest.* 111: 217–223.
- Han, B., P. Serra, A. Amrani, J. Yamanouchi, A. F. M. Marée, L. Edelstein-Keshet, and P. Santamaria. 2005. Prevention of diabetes by manipulation of anti-IGRP autoimmunity: high efficiency of a low-affinity peptide. *Nat. Med.* 11: 645–652.
- Amrani, A., J. Verdager, P. Serra, S. Tafuro, R. Tan, and P. Santamaria. 2000. Progression of autoimmune diabetes driven by avidity maturation of a T-cell population. *Nature* 406: 739–742.
- Liblau, R. S., F. S. Wong, L. T. Mars, and P. Santamaria. 2002. Autoreactive CD8 T cells in organ-specific autoimmunity: emerging targets for therapeutic intervention. *Immunity* 17: 1–6.
- Aichele, P., D. Kyburz, P. S. Ohashi, B. Odermatt, R. M. Zinkernagel, H. Hengartner, and H. Pircher. 1994. Peptide-induced T-cell tolerance to prevent autoimmune diabetes in a transgenic mouse model. *Proc. Natl. Acad. Sci. USA* 91: 444–448.
- Marée, A. F. M., P. Santamaria, and L. Edelstein-Keshet. 2006. Modeling competition among autoreactive CD8⁺ T cells in autoimmune diabetes: implications for antigen-specific therapy. *Int. Immunol.* 18: 1067–1077.
- Khadra, A., P. Santamaria, and L. Edelstein-Keshet. 2009. The role of low avidity T cells in the protection against type 1 diabetes: a modeling investigation. *J. Theor. Biol.* 256: 126–141.
- Tsai, S., A. Shameli, J. Yamanouchi, X. Clemente-Casares, J. Wang, P. Serra, Y. Yang, Z. Medarova, A. Moore, and P. Santamaria. 2010. Reversal of autoimmunity by boosting memory-like autoregulatory T cells. *Immunity* 32: 568–580.
- Moore, A., J. Grimm, B. Han, and P. Santamaria. 2004. Tracking the recruitment of diabetogenic CD8⁺ T-cells to the pancreas in real time. *Diabetes* 53: 1459–1466.
- Khadra, A., P. Santamaria, and L. Edelstein-Keshet. 2010. The pathogenicity of self-antigen decreases at high levels of autoantigenicity: a computational approach. *Int. Immunol.* 22: 571–582.
- De Boer, R. J., and A. S. Perelson. 1994. T cell repertoires and competitive exclusion. *J. Theor. Biol.* 169: 375–390.
- Kurrer, M. O., S. V. Pakala, H. L. Hanson, and J. D. Katz. 1997. Beta cell apoptosis in T cell-mediated autoimmune diabetes. *Proc. Natl. Acad. Sci. USA* 94: 213–218. β
- Mahaffy, J. M., and L. Edelstein-Keshet. 2007. Modeling cyclic waves of circulating T-cells in autoimmune diabetes. *SIAM J. Appl. Math.* 67: 915–937.
- Penaranda, C., and J. A. Bluestone. 2009. Is antigen specificity of autoreactive T cells the key to islet entry? *Immunity* 31: 534–536.